Solid State Ionics 417 (2024) 116706

Contents lists available at ScienceDirect

Solid State Ionics

journal homepage: www.elsevier.com/locate/ssi

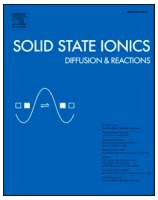

Quantitative determination of charge trapped at grain boundaries in ionic conductors by impedance spectroscopy

Sangtae Kim [a,1], Sergey Khodorov [b], Leonid Chernyak [c], Thomas Defferriere [d], Harry Tuller [d], Igor Lubomirsky [b,*]

[a] Department of Materials Science and Engineering, University of California, Davis, USA
[b] Department of Molecular Chemistry and Materials Science, Weizmann Institute of Science, USA
[c] Department of Physics, University Central Florida, Florida, USA
[d] Department of Materials Science and Engineering, Massachusetts Institute of Technology, USA

ARTICLE INFO

Keywords:
Ionic conductivity
Grain boundaries
Impedance spectroscopy
Space charge
Linear diffusion model
I-V curves

ABSTRACT

We propose a method for determining the density of space charge trapped at grain boundaries in polycrystalline solid state ionic conductors. The method is an extension of the earlier proposed Linear Diffusion Model (LDM) that relies on the impedance spectra-derived current-voltage characteristics of grain boundaries. The utility of the extended LDM version is demonstrated to successfully and nondestructively obtain values for the space charge density trapped at the grain boundaries in a variety of oxygen ion conductors including Sr-doped $LaGaO_3$, Y-doped CeO_2, and Gd-doped CeO_2, and proton conductors including Sr-doped $LaNbO_3$ and Y-doped $BaZrO_3$. For all cases, the density of the space charge trapped at the grain boundaries was $<0.2 C/m^2$, corresponding to a fraction of electron charge per unit cell. The proposed technique, while it lacks the ability to determine the thickness of the grain boundary core when much smaller than the Debye length, it can be used to distinguish between space charge vs insulating layer contributions to the grain boundary resistance.

1. Introduction

Grain boundaries in polycrystalline solid ionic conductors typically occupy only a small volume fraction of the solid. However, they often play a crucial role in influencing the overall electrical resistivity [1–3]. This phenomenon is particularly evident in oxygen-ion and proton conductors, which are fundamental components of solid oxide ion based fuel/electrolysis cells [1,4–7], technologies considered vital for future clean energy needs. Gaining a comprehensive understanding of grain boundary resistivity in oxygen and proton-conducting ceramics is therefore paramount [8,9]. The complexity of the issue is heightened by the fact that grain boundary resistance in a given material may stem from various sources, making the nature and source of grain boundary resistance a subject of intense debate in the field of *Solid State Ionics* [10–12].

Interpreting grain boundary resistance presents a significant challenge since, in addition to electrical interactions, various other contributions have been proposed [10–17]. Grain boundary resistance reportedly can have two distinct contributions: (i) charge trapped in the grain boundary core, causing a space charge region in the adjacent grain (Fig. 1) [1,4–6,8,9,18–23], and (ii) physical obstructions due to insulating secondary phases or disordered layers [19,20]. While advanced Transmission Electron Microscopy (TEM and TEM holography) techniques [19–22,24] can often provide important information about specific grain boundaries, they are limited in being able to provide an overall picture of the broad distribution of grain boundaries that are found in typical polycrystalline ceramics. This is exacerbated by the fact that it is not clear whether the selected interfaces studied by TEM are representative of the actual current paths taken by the ions. As such, developing macroscopic methods that enable one to directly quantify the properties of grain boundary interfaces relevant to the charge transport path is vital for the systematic interpretation of their influence on performance. In the following, we discuss how impedance spectroscopy data, and their analysis by the linear diffusion model (LDM), can be used to obtain a clearer understanding of the sources of grain boundary resistance in given solid electrolyte materials.

We begin by considering the case in which the grain boundary resistance is dominated by space charge barriers. Based on the Schottky

* Corresponding author.
E-mail address: igor.lubomirsky@weizmann.ac.il (I. Lubomirsky).
[1] Deceased.

https://doi.org/10.1016/j.ssi.2024.116706
Received 22 July 2024; Received in revised form 11 September 2024; Accepted 17 September 2024
Available online 28 September 2024

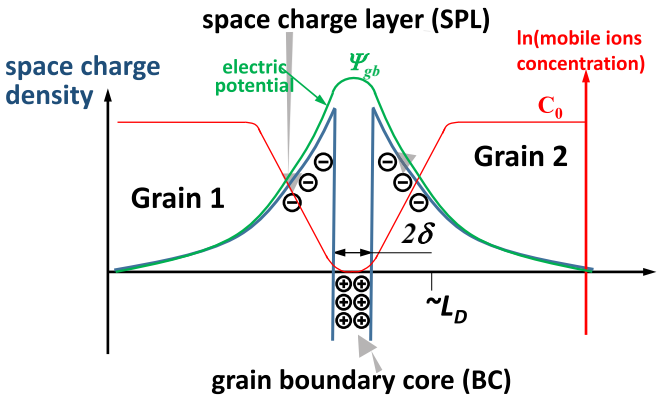

Fig. 1. Schematic of charge distribution in a grain boundary: charge trapped in grain boundary core (BC) repels mobile ions forming a space charge depleted of charge carriers. The thickness of the space charge layer is at least a few L_D, much larger than the thickness of the core, d_{real}, usually only one or two atomic layers thick. The scheme is given for the case of positive charge carriers and positive charge trapped, while the immobile dopants are negatively charged. This corresponds to the cases considered in this work. Reversal of the sign of the charge does not affect the results of the calculation. The maximum value of the potential, Ψ_{gb}, is the grain boundary potential.

formalism applied to grain boundaries in polycrystalline ionic conductors [25], Maier and Fleig [26] proposed a method (hereafter RR method) to determine the grain boundary potential based on the ratio of grain boundary to bulk resistivity. The RR method requires an impedance spectrum with clearly identifiable RC elements representing contributions from both grain boundaries and grain interiors. We subsequently developed an alternative approach, the linear diffusion model (LDM), which provides a more accurate quantitative determination of the grain boundary potential [15,27–32]. Although requiring multiple impedance spectra, LDM can reliably differentiate between contributions from space charge-induced grain boundary resistance versus those arising from physical obstructions [30].

The main objective of the current work is to show that the extended LDM models allows one to accurately determine the grain boundary potential, as well as the density of trapped states within the grain boundary cores, the latter not accessible via the RR methods.

2. Linear diffusion model (LDM)

The LDM was initially designed to explain the cause of the current-voltage characteristics (I-V curves) of grain boundaries in polycrystalline solid state ionic conductors. The process of extracting the I-V curves from impedance spectra is well established. It necessitates the acquisition of impedance spectra under constant bias and subsequent analysis of changes incurred by bias to the RC-elements corresponding to the grain boundaries (see, for example, Fig. 4 in ref. [33] and the subsequent application of this technique in [27–32,34]).

The LDM is based on a set of four assumptions, the applicability of which were previously discussed [27–32]:

(a) The charges in the grain boundary core are permanently trapped and are not influence by applied field.

(b) The grain boundary charge, Q_{gb}, is concentrated in the grain core, with half-thickness of d. We approximate the charge distribution as a Gaussian function; however, the exact shape does not affect the field distribution if d is no larger than the Debye length:

$$L_D = \sqrt{\frac{\varepsilon \cdot \varepsilon_0 \cdot k_B \cdot T}{(z \cdot q)^2 \cdot C_0}} \tag{1}$$

where q is the elemental charge, z the relative charge of the mobile ions, ε the dielectric permittivity, ε_0 the dielectric permittivity of vacuum and C_0 the concentration of mobile ions in the grain interiors.

c) The diffusion coefficient D of the mobile ions remains fixed within both the grain interiors and grain boundaries for a given temperature and doping level. The blocking of ionic current flux results from the induced electric field, due to the presence of the trapped charge at the grain boundary, given by the spatial distribution $n_{gb}(x)$. This assumption, however, is valid only for the case of grain boundaries being free of contaminants and disordered layers. It is important to emphasize, however, that the LDM is also valid for cases of contaminated grain boundaries and, in conjunction with the RR method, is capable of separating space charge contributions to the grain boundary resistance from other sources. This case was considered in detail in Ref. [30].

d) All species are assumed to follow Boltzmann statistics, which allows the ionic mobility, μ, to be related to the diffusion coefficient, D, via the Einstein-Smoluchowski equation $\mu = D/V_{th}$, (where)

$$V_{th} = k \cdot T/(z \cdot q) \tag{2}$$

is the thermal voltage. This assumption is somewhat controversial given that most ionic conductors cannot be treated as dilute solutions with perfectly independent moving ions (more sophisticated treatments can be found in refs [10–16]). However, the assumption of a Boltzmann distribution is sufficient for the LDM to yield a set of practically important and easily verifiable predictions based on the numerical solution of the well-known transport Eq. [35–37]. It relates the electric field, ϕ, current density, j, and density of trapped charge $n_{gb}(x)$:

$$\phi''(x) - \left(\phi'(x) - 1 + n_{gb}(x)\right) \cdot \phi(x) + \frac{\partial (n_{gb}(x))}{\partial x} - j = 0 \tag{3}$$

For practical purposes, this equation is given in dimensionless form. The normalization constants are:

(i) distance given in units of Debye length (Eq. (1));

(ii) electric field given in units of $E_0 = V_{th}/L_D$;

(iii) current density given in units of $J_0 = \frac{D}{L_D} C_0 \cdot z \cdot q$;

(iv) trapped charge density given in units of C_0 and expressed as $n_{gb}(x) = \frac{a}{\delta\sqrt{\pi}} exp\left(-(x/\delta)^2\right)$, (where)

$$a = \frac{Q_{gb}}{C_0 \cdot q \cdot z \cdot L_D} = \frac{Q_{gb}}{\sqrt{C_0 \cdot \varepsilon \cdot \varepsilon_0 \cdot C_0 \cdot T}} \text{ and } \delta = d \Big/ L_D \tag{4}$$

a &δ being the two values defining the grain boundary in dimensionless units, corresponding to Q_{gb}, and d in real dimensions. To avoid the problem of considering the interface between electrodes and ionic conductors, we considered an infinite chain of identical grains of length, l. Then the boundary conditions have a simple form of constraints requiring continuity of electric field and its derivative between the grains: $\phi(0) = \phi(l)$ and $\phi'(0) = \phi'(l)$, where l is the length of the grain and the grain boundary can be positioned anywhere within $[0; l]$ interval. Numerical solutions of Eq. (3) give three very specific experimentally verified predictions:

1. If plotted in coordinates ln (current) vs ln (U_{gb}/V_{th}), I-V curves have at least two distinct linear regions (Fig. 3). For $U_{gb}/V_{th} < 1$, the slope of the I-V curves is strictly 1, which implies that current is directly proportional to applied voltage: $I \propto U_{gb}$. Thus, LDM predicts that at low voltages, GBs behaves as resistors, i.e., an "Ohmic" regime. Above a transition region at $1 < U_{gb}/V_{th} < 10$, increase in applied voltage results in the appearance of a second linear region on the log-log plot. This second linear region at $10 < U_{gb}/V_{th} < 80$ has a slope, n, larger than 1, so that the current is proportional to a power of applied voltage: $I \propto U_{gb}^n$, a "super-Ohmic" regime (Fig. 3). For higher voltages, the charge trapped in the grain boundary may be fully compensated by the ionic current, i.e., the amount of charge injected becomes larger than the charge trapped in the grain boundary core (see Fig. 2c in ref. [31]. Then, the I-V curve becomes again Ohmic, $I \propto U_{gb}$. This is a relatively rare, but possible case (see for instance section 4.4). The overall resistance of the sample in this regime is then defined by part of the grain boundary resistance not

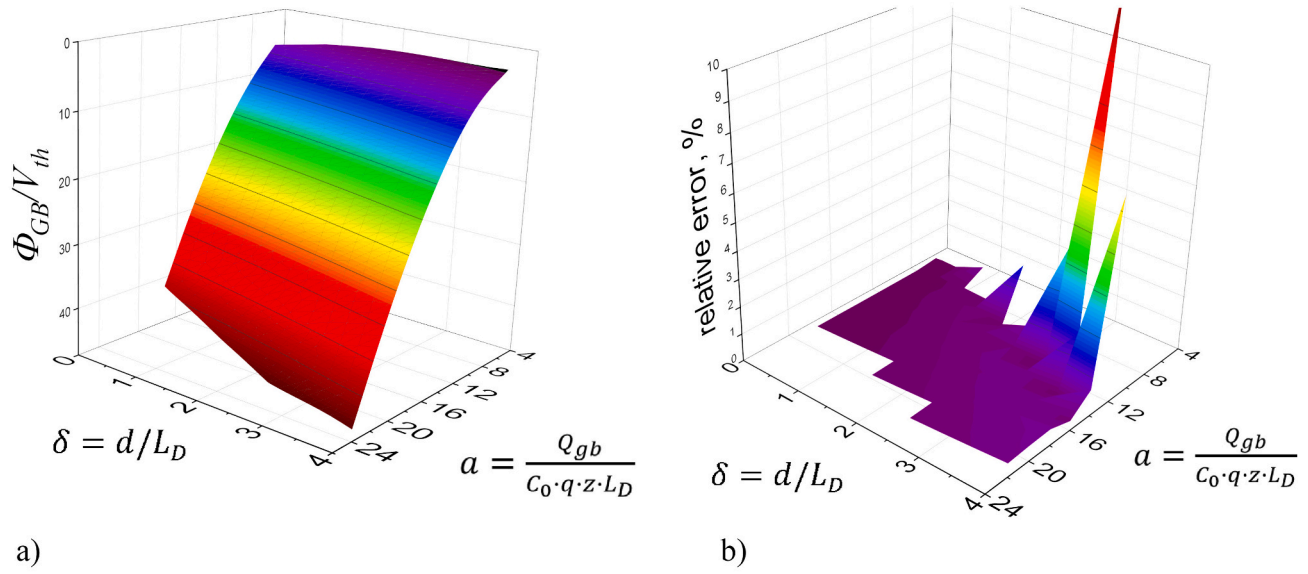

Fig. 2. (a) Values of the grain boundary potential in dimensionless units $\varphi_{gb} = \Psi_{gb}/V_{th}$ as a function of normalized grain boundary charge, a, and grain boundary core thickness $\delta = d/L_D$. The surface is smooth, allowing it to be approximated locally in quadratic form. (b) the relative error of fit to (7), for small values of δ, φ_{gb}.

related to space charge and by the resistance of the grain interior (bulk). **2.** The slope, n, of the super-Ohmic region ($I \propto U_{gb}^n$) is directly related to the value of the grain boundary potential of the super-Ohmic region [31]:

$$\varphi_{gb} = \Psi_{gb}/V_{th} = n/f_{KL} \tag{5}$$

where $f_{KL} = 0.41$ ($\sim[\sqrt{2} - 1]$) is a previously determined empirical factor [31]. It was obtained by plotting the slope of the super-Ohmic regime of the simulated I-V curves against the grain boundary potential, expressed in units of the thermal voltage (V_{th}). The factor remains constant across the practically important range of grain boundary potentials (in units of V_{th}), from approximately 2 to at least 40, regardless of the values of Q and d, as long as a given pair of Q and d results in the same grain boundary potential.

3. If no significant release of trapped space charge occurs, the slope n decreases with temperature as

$$Crit = T \cdot (n - f_{KL}) = const. \tag{6}$$

This criterion also implies that the absolute values of the grain boundary potential, Ψ_{gb}, remain constant with temperature, while the value of φ_{gb} decreases as 1/T because $V_{th} \sim$T. If the condition holds ($Crit = const$), LDM is valid and Eq. (5) can be used to determine the grain boundary potential.

While the LDM based on Eq. (3) has been highly successful in explaining the I-V curves of grain boundaries and extracting values of the grain boundary potential, it has, until now, faced challenges in extracting the values of Q_{gb} and d. This limitation arises from the fact that Eq. (3) cannot be solved analytically. For a given material, each pair of Q_{gb} and d leads to a well-defined value of the grain boundary potential Ψ_{gb}. However, Ψ_{gb} at a given temperature may correspond to an infinitely large number of pairs Q_{gb} and d. Therefore, determining Ψ_{gb} from one set of Q_{gb} and d is an ill-posed task. Nevertheless, as we demonstrate below, by using a set of values determined at different temperatures, this task becomes achievable.

3. Mathematical background

Solving Eq. (3) numerically for the practically important values of a and δ in dimensionless space produces a smooth (all derivatives are continuous) surface $\varphi_{gb}(a, \delta)$ (Table 1, Fig. 2a), which implies that $\varphi_{gb}(a, d)$ can be approximated locally in quadratic form. Indeed, fitting the surface with Matlab leads to the expression:

$$\varphi_{gb}(a, d) = \frac{\Psi_{gb}}{V_{th}} = S \cdot a \cdot \delta + B \cdot a^2 + 1 \tag{7}$$

where

$$S = -0.282 \left(\text{i.e.} \frac{1}{\sqrt{4\pi}}\right) \text{ and } B = 0.125 \tag{8}$$

(i.e. 1/8) are empirical dimensionless constants.

For values of the grain boundary potential $\Psi_{gb} > 4V_{th}$, the accuracy of the fit is better than 1 % (Fig. 2a, Table 1). The accuracy deteriorates for the cases if $\Psi_{gb} < 4V_{th}$ (Fig. 1b) corresponding to small values of trapped charge Q_{gb} and large thicknesses of the grain boundary core

Table 1
Values of φ_{gb} as a function of a and d obtained by solving Eq. (3) numerically as described in ref. [31].

$a \backslash d$	4.0	3.5	3.0	2.5	2.0	1.5	1.0	0.5	0.3	0.1
6.0							3.8	4.7	5.1	5.3
8.0	2.0	2.4	3.0	3.7	4.6	5.6	6.7	7.9	8.4	8.7
10.0	3.4	4.3	5.3	6.5	7.9	9.3	10.7	12.1	12.8	13.1
12.0	6.0	7.4	8.9	10.6	12.2	13.9	15.6	17.3	18.2	18.6
14.0	9.9	11.8	13.7	15.6	17.6	19.6	21.6	23.5	24.5	25.0
16.0	15.0	17.2	19.5	21.7	24.0	26.2	28.5	30.7	31.9	32.4
18.0	21.2	23.7	26.3	28.8	31.3	33.9	36.4	39.0	40.2	40.9
20.0	28.4	31.3	34.1	36.9	39.7	42.5				
22.0	36.7	39.8	42.9	46.0						

(few L_D). These cases, however, are of little practical interest because they occur if Q_{gb} is small in comparison to the bulk carrier concentration and/or is distributed over a large distance, $\delta > L_D$ (Table 1). For these cases, the resistance of the grain boundaries does not contribute significantly to the overall resistance of a given sample. The quadratic form of Eq. (7) can be rewritten using the explicit values for a and δ:

$$a\cdot\delta = \frac{Q_{gb}\cdot d}{T}\frac{z\cdot q}{\varepsilon\cdot\varepsilon_0\cdot k} \text{ and } a^2 = \frac{Q_{gb}^2}{T}\frac{1}{C_0\cdot\varepsilon\cdot\varepsilon_0\cdot k} \tag{9}$$

The first multiplier in these expressions contains the variables describing the grain boundaries and the second multiplier depends only on the properties of the material: z-charge of the charge carriers, C_0-concentration of the charge carriers in bulk and ε is dielectric permittivity. For a given material these parameters are known and can be abbreviated as constants:

$$C_1 = \frac{z\cdot q}{\varepsilon\cdot\varepsilon_0\cdot k} \text{ and } C_2 = \frac{1}{C_0\cdot\varepsilon\cdot\varepsilon_0\cdot k}. \tag{10}$$

Then the grain boundary potential in real dimensions looks as:

$$\frac{\Phi_{gb}}{V_{th}} = S\cdot C_1\frac{Q_{gb}\cdot d}{T} + B\cdot C_2\frac{Q_{gb}^2}{T} + 1, \tag{11}$$

At a given temperature, this is an equation with two variables Q_{gb} and d. Since $\frac{\Phi_{gb}}{V_{th}}$ can be determined directly from the impedance spectroscopy data as the slope of the I-V curves (an example in Fig. 3), $d\left(ln\left(I_{gb}\right)\right)/d\left(ln\left(U_{gb}\right)\right) = n = f_{KL}\frac{\Phi_{gb}}{V_{th}}$, Eq. (11) allows the determination of Q_{gb} and d if the impedance spectroscopy measurements are performed at two or more temperatures using a standard least squares method (LSM). The quality of the data for this procedure is defined by the criteria in Eq. (6), demanding that Q_{gb} and d not change with temperature.

One has to note that for $d<<L_D$, the I-V curves and the grain boundary potential do not depend on values of d (Eq. (11), Table 1, Fig. 2). Therefore, as an approximation for $d<<L_D$ one can take:

$$Q_{gb\_appr} = \sqrt{\left(\frac{\Phi_{gb}}{V_{th}} - 1\right)\cdot\frac{1}{B\cdot C_2}}\cdot T = \sqrt{8\cdot T\cdot C_0\cdot\varepsilon\cdot\varepsilon_0\cdot k\cdot(n/f_{kl} - 1)} \tag{12}$$

Even though this equation allows determination of the charge density trapped at the grain boundaries using only an I-V curve acquired at a single temperature, it is limited to the condition, $d<<L_D$, which while highly common (see below), is not always satisfied. Moreover, Q_{gb_appr} is valid only if the criterion given in Eq. (6) is fulfilled. Therefore, measurements conducted at a minimum of two different temperatures, are necessary. An additional utility of Q_{gb_appr} is that it can serve as an initial approximation while performing LSM-fitting on the data at multiple temperatures.

4. Practical implementation

To illustrate, we have applied this approach to the data that we previously published within the framework of the development of the LDM.

4.1. Case 1: 1 Mol% Sr doped $LaGaO_3$

We begin with the case of the oxygen ion conductor 1 mol% Sr doped $LaGaO_3$ (LSG1) considered in ref. [28] with $\varepsilon \approx 26$ [38], $z = 2$, volume of unit cell $Vol = 0.236\ nm^3$ [39], concentration of oxygen vacancies $C_0 = 2.55\cdot10^{20}\ cm^{-3}$ and L_D within the range of 0.25 nm (250 °C) to 0.275 nm (350 °C), less than a unit cell size. LSG1 is viewed as one of the rare materials in which the current across the grain boundary has been verified to be exclusively limited by space charge. For this material, the values of the grain boundary potential determined with RR and LDM match perfectly (Fig, 4 in ref. [28]). The value of *Crit*, calculated with Eq. (6), varies by less than 2 % in the measured temperature range, indicating that all five points are suitable for analysis. From the physical parameters of the material, one obtains $C_1 = 1.08\cdot10^{14}\ \frac{m\cdot K}{C}$ and $C_2 = 1.24\cdot10^6\left(\frac{m^2}{C}\right)^2 K$. The approximated value for $Q_{gb_{appr}} = 0.165\frac{C}{m^2}$, according to Eq. (12), for all temperatures, with values of *Crit* (Fig. 3b) varying less that 1.6 % between 250 °C and 350 °C, indicating that no trapped charge is released within this temperature range. The LSM yields an excellent fit for $Q_{gb} = 0.166\frac{C}{m^2} \approx Q_{gb_{appr}}$ and $d<<L_D$. An analysis of Eq. (11) with this value of $Q_{gb} = 0.166\frac{C}{m^2}$, shows that the first term becomes <10 % of the second term already for $d = 0.1$ nm. Therefore, the fact that the best fit is achieved for $d \longrightarrow 0$, strongly suggests that the trapped charge is confined to one atomic plane. As a way to visualize the charge distribution, one can consider the average concentration of charge per unit cell as $\sigma_{unit} \approx Q_{gb}\cdot Vol^{2/3}/q = 0.19$ electron charge per unit cell at the interface between two neighboring grains (Fig. 1). The approximation of $Vol^{2/3}$ for the "area of the unit cell cross section" is used because $LaGaO_3$ is not cubic.

4.2. Case 2: 1 Mol% Y doped CeO_2

The case of 1 mol% Y doped CeO_2 (YCO1) was considered in ref. [31] (Fig. 4a). YCO1 is an oxygen ion conductor like LSG1 ($z = 2$). For this material $\varepsilon \approx 24$, unit cell size 0.541 nm, and $C_0 = 2.23\cdot10^{20}\cdot cm^{-3}$. The constants in Eq. (11) are calculated to be $C_1 = 1.09\cdot10^{14}\ \frac{m\cdot K}{C}$ and $C_2 =$

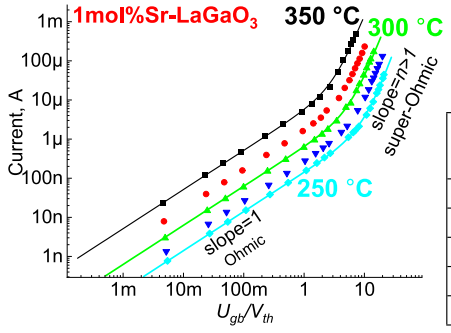

a)

T, °C	T,K	n	Crit	φ_{gb} exp	φ_{gb} fit	deviation, %	a
250	523	3.87	1.80	9.21	9.10	1.3	15.5
275	538	3.68	1.80	8.76	8.73	0.4	15.2
300	573	3.51	1.77	8.36	8.40	0.4	14.8
325	598	3.38	1.77	8.05	8.09	0.4	14.5
350	623	3.23	1.75	7.70	7.80	4.9	14.2

b)

Fig. 3. (a) Experimental I-V curves for 1 mol% Sr-doped **$LaGaO_3$** from ref. [28] the continuous curves are simulated for $\boldsymbol{Q_{gb} = 0.166\ C/m^2}$ and $\boldsymbol{d} = 0.01$ nm (b) The experimental values of $\boldsymbol{n}$ for various temperatures, grain boundary potential in units of $\boldsymbol{\varphi_{gb} = \frac{\Phi_{gb}}{V_{th}}}$, with best fit values and deviation of the best fit values from experimental data. The fit is not sensitive to the value of d, leading to $\boldsymbol{d} < 0.05$ nm ($\boldsymbol{\delta << L_D}$). $\boldsymbol{\Psi_{gb}}$ for the whole temperature range remains constant 207 ± 1 mV, as predicted by LDM

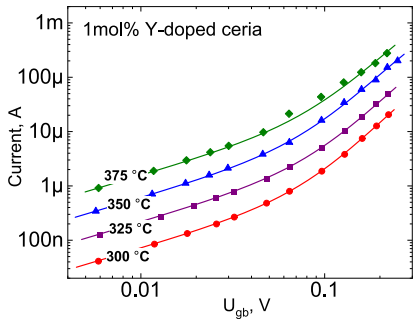

a)

T, °C	T,K	n	Crit	φ_{gb} exp	φ_{gb} fit	deviation, %	a
300	573	2.85	1.40	6.95	6.95	<0.1	6.9
325	598	2.75	1.40	6.71	6.70	0.1	6.8
350	623	2.65	1.40	6.46	6.47	0.13	6.6
375	648	2.25	1.2	5.49	N/A	N/A	6.5

b)

Fig. 4. (a) Experimental I-V curves for 1 mol% Y-doped ceria from Ref. [31] The continuous curves are simulated for $\boldsymbol{Q_{gb} = 0.141\ C/m^2}$ and $\boldsymbol{d} = 0.01$ nm; (b) The experimental values of $\boldsymbol{n}$ for various temperatures, grain boundary potential in the units of $\boldsymbol{\varphi_{gb} = \frac{\Phi_{gb}}{V_{th}}}$, the best fit values and the deviation of the best fit value from the experimental data. The fit is not sensitive the value of d leading to $\boldsymbol{d} < 0.01$ nm ($\boldsymbol{\delta << L_D}$, which for this case only 0.15 nm, i.e. < than 1/3rd unit cell). $\boldsymbol{\Psi_{gb}}$ for the 300–350 °C temperature range is 173 ± 1 mV.

$1.35{\cdot}10^6 \left(\frac{m^2}{C}\right)^2 K$. The measurements were performed at 300, 325, 350 and 375 °C; at all temperatures the I-V curves followed the predictions of LDM with both Ohmic and super-Ohmic regimes visible (Fig. 4a). The values of *Crit*, however, remain nearly constant for the first three temperatures (300, 325, 350 °C) with less than 0.2 % spread, while at 375 °C the value of *Crit* changes by ≈ 15 % indicating that at this temperature some trapped charge is released (Fig. 4b). For the first three points the initial approximation for the density of the trapped charge is $Q_{gb_{appr}} = 0.142 \frac{C}{m^2}$. LSM fitting to the first three temperature points also suggests that $Q_{gb} = Q_{gb_{appr}} = 0.142 \frac{C}{m^2}$ and $d << L_D$. The value of L_D at these temperatures is ≈ 0.26 nm, which is about half of a unit cell, leading to the suggestion that the space charge is trapped within one monolayer between the grains with the density $\sigma_{unit} = 0.13$ electrons per unit cell.

4.3. Case 3: The effect of contaminants on grain boundary properties

It is of a particular interest to examine the approach described above to a grain boundary contaminated by a second phase described in ref. [30]: 3 mol% Gd-doped CeO_2 (GDC3) contaminated with 500 ppm of SiO_2 precipitated at the grain boundaries (Fig. 5a). For this case, the main contribution to the grain boundary resistance does not come from the space charge. Indeed, there is a large difference between the grain boundary potential calculated using the RR and LDM models (130 mV according to LDM and 500 mV according to RR [30]). The concentration of mobile charge carriers for 3GDC is higher $C_0 = 7.58{\cdot}10^{20}{\cdot}cm^{-3}$, C_1 is the same and $C_2 = 4.45{\cdot}10^5 \left(\frac{m^2}{C}\right)^2 K$, is smaller than that for YCO1, respectively. The difference in the value of *Crit* are less than 4 % between all temperatures examined (325 °C to 400 °C), which implies that all the points are to be included in the optimization. A higher concentration of charged carriers leads to a much smaller Debye length, 0.15–0.16 nm; nevertheless the LSM optimization indicates that the best fit is obtained for $Q_{gb} = Q_{gb_{appr}} = 0.21 \frac{C}{m^2}$ and $d << L_D$, with the difference between the simulated and the actual values of φ_{gb} less than 3 % (Fig. 5b). Apparently, SiO_2 precipitating at the grain boundaries does not decrease the space charge density, as it is ≈ 0.2 electron charge per unit cell for case with SiO_2, which is even higher that for YCO1 (section 4.2).

4.4. Case 4: Grain boundary of proton conductor Sr-doped $LaNbO_4$

Analyzing a grain boundary for proton conductors is more difficult because the concentration of mobile ions in proton conductors which depends on the degree of hydration, is not known precisely, even in the case when thermal gravimetric analysis is performed (see for instance [40,41]). This poses a problem of knowing the values of C_0 and, therefore, L_D. Another problem is that proton transport across grain boundaries is very sensitive to factors other than space charge (see refs [42–46] for $BaZrO_3$ and refs. [47] [48,49] for Sr-doped $LaNbO_4$). In the example of 0.5 mol% Sr-doped $LaNbO_4$ given in our earlier work [29], the second Ohmic region in the I-V curves is observed (Fig. 6a). This is the region in which the space charge at the grain boundaries is completely compensated by injected charge carriers (see the LDM analysis of this case in ref. [31]) and the current is limited by other factors, proving that the main contribution to the grain boundary resistance is not defined by the space charge [30,31]. The difference between the values of the grain boundary

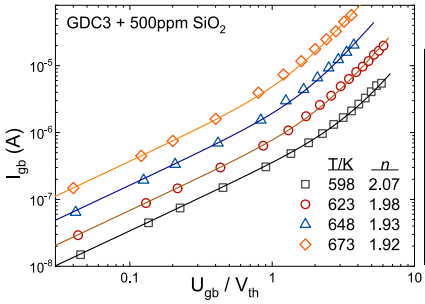

a)

T, °C	T,K	n	Crit	φ_{gb} exp	φ_{gb} fit	deviation, %	a
325	598	2.07	1.04	5.22	5.09	-2.4	5.7
350	623	1.98	0.98	4.83	4.93	2.0	5.6
375	648	1.93	0.98	4.71	4.77	1.4	5.5
400	673	1.92	1.02	4.68	4.63	-1.0	5.4

b)

Fig. 5. (a) Experimental I-V curves for 3 mol% Gd-doped CeO_2 with deliberately introduced 500 ppm of SiO_2 precipitated at grain boundaries from ref. [30]. The continuous lines are simulated for $Q_{gb} = 0.21\ C/m^2$ and d=0.01 nm. (b) The experimental values of n for various temperatures, grain boundary potential in the units of $\varphi_{gb} = \frac{\Phi_{gb}}{V_{th}}$, the best fit values and the deviation of the best fit value from the experimental data. Ψ_{gb} for the whole temperature range is 129 ± 5 mV.

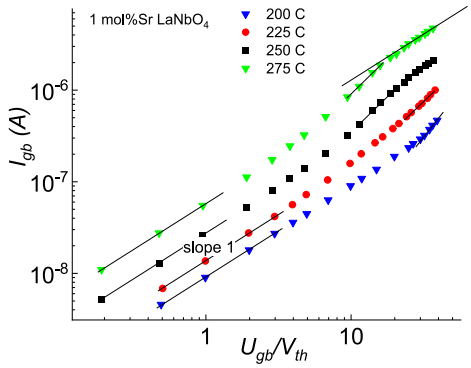

a)

T, °C	T,K	n	$Crit$	φ_{gb} exp	φ_{gb} fit	deviation, %	a
200	473	1.77	0.64	4.2	4.2	-1.3	5.0
225	498	1.7	0.64	4.0	4.0	-1.1	4.9
250	523	1.6	0.62	3.8	3.9	1.3	4.8
275	548	1.54	0.61	3.7	3.7	1.7	4.7

b)

Fig. 6. (a) Experimental I-V curves for 1 mol% Sr-doped $LaNbO_3$, the data form ref. [29]. If full hydration is assumed, the best fit is achieved for $Q_{gb} = 0.04\ C/m^2$ and $d << 0.01\ L_D$ nm. (b) The experimental values of n for various temperatures, grain boundary potential in the units of $\varphi_{gb} = \frac{\Phi_{gb}}{V_{th}}$, the best fit values and the deviation of the best fit value from the experimental data. Ψ_{gb} for the whole temperature range remains constant 86 ± 0.5 mV, as predicted by LDM

potential derived by the RR method (>0.6 V) and with the LDM (<0.2 V) are particularly large (see Fig. 4 in ref. [29]). Nevertheless, the slopes "n" for the sample follow the behavior of LDM near perfectly: with *Crit* values differing only ~2 % for the whole temperature range, indicating that the charged trapped at the grain boundaries is not released by heating from 200 °C to 275 °C (this case is in detail considered in ref. [30]). Calculating Q_{gb} using Eq. (11) or even obtaining approximate values using Eq. (12), requires the value of C_0, which is unknown. However, since $Q_{gb_{appr}} \propto \sqrt{C_0}$, one can make a useful estimate. If the material (z = 1, ε=20, $Vol = 0.34\ nm^3$) is assumed to be fully hydrated, then $C_0 = 5.9{\cdot}10^{-19}\ cm^{-3}$, $Q_{gb_{appr}} = Q_{gb} = 0.0415\ \frac{C}{m^2}$ with d < $<L_D$. This clearly indicates that even if the material is fully hydrated, the charge density at the grain boundaries is much smaller than for the case of oxygen ion conductors. Assumption of only 5 % hydration reduces the value of Q_{gb} by a factor $\sqrt{20} \approx 4.5$ to $0.0093\ \frac{C}{m^2}$.

4.5. Case 5: Grain boundary of proton conductor 2 mol% Y-doped $BaZrO_3$

Y-doped $BaZrO_3$, mentioned in ref. [32], presents the most difficult case for analysis because even though the shape of the I-V curves follows the predictions of the LDM (Fig. 7), the value of *Crit* is not constant. This suggests that the trapped charge at the grain boundaries is not constant within this temperature range. Moreover, the value of the slope does not decrease with temperature, it increases, with the simplest explanation that some water loss occurs, leading to a decrease in proton concentration and, thereby, an increase in the grain boundary potential (see the analysis based on the hydration energy in ref. [32]). This limits the quantitative applicability of the LDM model. However, some conclusions can still be made since the I-V curves clearly show both Ohmic and super-Ohmic regions.

(i) The difference between the grain boundary potential estimated using the LDM and RR methods is particularly large: LDM predicts 0.3–0.4 V, while RR predicts nearly 1 V (see Fig. 7 in ref. [32] and refs. [45,50]) indicating that the major contribution to the grain boundary resistance does not come from the space charge.

(ii) The data in ref. [32] (Fig. 7) were collected after hydration at 300 °C for a prolong period of time (more than four weeks and a very small samples was used 1.3 × 2.2 × 0.2 mm^3), which suggests that the initial degree of hydration was close to 100 %. This leads to $Q_{gb_{appr}} = 0.15\ C/m^2$. According to the thermodynamic data (see Fig. 3b in ref. [32] calculated on the basis of the thermodynamic data in ref. [51]), the degree of hydration at 450 °C is expected to drop to ≈ 72 %, which, if used to calculate $Q_{gb_{appr}}$, again yields the same value of $0.15\ C/m^2$. This strongly suggests the trapped charge at the grain boundaries undergoes only minor changes even though a considerable water loss takes place. Moreover, even though the space charge is non-negligible, it is not the main contributor to the grain boundary resistance.

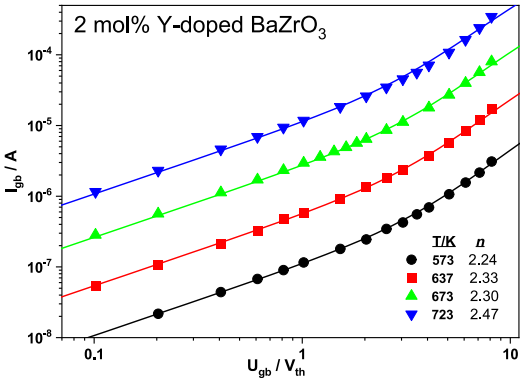

a)

T, °C	T,K	n	$Crit$	φ_{gb} exp
300	573	2.24	1.04	5.33
364	637	2.33	1.22	5.55
400	673	2.3	1.26	5.48
450	723	2.47	1.48	5.88

b)

Fig. 7. (a) Experimental I-V curves for 2 mol% Y-doped $BaZrO_3$ from ref. [32]. The continuous lines are given for guidance only. No simulation is possible because the concentration of protons varies with temperature. (b) The experimental values of n for various temperatures, grain boundary potential in the units of $\varphi_{gb} = \frac{\Phi_{gb}}{V_{th}}$. Eq. (5) used given *Crit* is not constant.

5. Concluding remarks

The analysis based on LDM is sufficient to make a quantitative estimate of the grain boundary characteristics. The accuracy of the space charge density estimate depends on a number of factors: (a) The quality of the impedance spectroscopy data and the accuracy of determining the slopes of the super-Ohmic regime "n". In general, these values have at least a few percent of uncertainty. (b) Changes in the trapped charge density as a function of temperature can be estimated using the value of *Crit* (Eq. (6)). Variations in these values impose a limit on the accuracy of the estimate. Apparently, these sources of the error are larger than the error in fitting the solutions (Eq. (7)). In this view, one safely assumes that the accuracy of the estimates of Q_{gb} for the cases 4.1 to 4.4 is better than 10 %.

Determination of the thickness of the grain boundary core by application of LDM is not possible, because unless $d \approx L_D$ or $d > L_D$, the grain boundary potential is only weakly dependent on the value of d. The analysis given above shows that for all materials reported, $d < L_D$ even if L_D is only a fraction of a unit cell.

In conclusion, one can emphasize the general utility of that the LDM-based method for determining the space charge trapped at the grain boundaries in ionic conductors non-destructively and without requirement of complex instrumentation.

CRediT authorship contribution statement

Sangtae Kim: Writing – original draft, Methodology, Investigation, Conceptualization. **Sergey Khodorov:** Visualization, Validation, Supervision, Software, Methodology, Formal analysis, Data curation, Conceptualization. **Leonid Chernyak:** Visualization, Investigation, Data curation. **Thomas Defferriere:** Writing – review & editing, Writing – original draft, Methodology, Formal analysis, Data curation. **Harry Tuller:** Writing – review & editing, Writing – original draft, Methodology, Formal analysis, Data curation. **Igor Lubomirsky:** Writing – review & editing, Writing – original draft, Visualization, Software, Formal analysis, Data curation, Conceptualization.

Declaration of competing interest

The authors declare that they have no known competing financial interests or personal relationships that could have appeared to influence the work reported in this paper.

Data availability

Data will be made available on request.

Acknowledgements

This work was supported by the US Army Research Office (ARO grant #W911NF2110263, I.L.) and by the Sagol Weizmann - MIT Bridge Program (award #143267). L.C. acknowledges support of the U.S. National Science Foundation (ECCS ##2310285, 2341747). TD and HT acknowledge partial support by the U.S. Department of Homeland Security, Countering Weapons of Mass Destruction Office, under awarded grant 22CWDARI00046. This support does not constitute an express or implied endorsement on the part of the US Government.

References

[1] J. Jamnik, J. Maier, Solid State Ionics 94 (1–4) (1997) 189.
[2] J. Maier, J. Eur. Ceram. Soc. 19 (6–7) (1999) 675.
[3] H.L. Tuller, Solid State Ionics 131 (1–2) (2000) 143.
[4] J. Jamnik, J. Maier, Berichte Der Bunsen-Gesellschaft-Physical Chemistry Chemical Physics 101 1 (1997) 23.
[5] J. Jamnik, J. Maier, J. Phys. Chem. Solids 59 (9) (1998) 1555.
[6] J. Jamnik, J. Maier, Solid State Ionics 119 (1–4) (1999) 191.
[7] X. Guo, W. Sigle, J. Maier, J. Am. Ceram. Soc. 86 (1) (2003) 77.
[8] X. Guo, J. Fleig, J. Maier, J. Electrochem. Soc. 148 (9) (2001) J50.
[9] X. Guo, J. Maier, J. Electrochem. Soc. 148 (3) (2001) E121.
[10] A.R. Genreith-Schriever, J.P. Parras, H.J. Heelweg, R.A. De Souza, Chemelectrochem 7 (23) (2020) 4718.
[11] A.L. Usler, R.A. De Souza, J. Electrochem. Soc. 168 (2021) 5.
[12] J.P. Parras, G. Feldmann, R.A. De Souza, J. Am. Ceram. Soc. 104 (11) (2021) 5946.
[13] B. Bandi, A. Chatterjee, Acta Mater. 240 (2022).
[14] R.A. De Souza, E.C. Dickey, Philosophical Transactions of the Royal Society a-Mathematical Physical and Engineering Sciences 377 (2019) 2152.
[15] R.A. De Souza, Z.A. Munir, S. Kim, M. Martin, Solid State Ionics 196 (1) (2011) 1.
[16] R.A. De Souza, Phys. Chem. Chem. Phys. 11 (43) (2009) 9939.
[17] Y.Y. Lin, A.X. Bin Yong, W.J. Gustafson, C.N. Reedy, E. Ertekin, J.A. Krogstad, N. H. Perry, Curr. Opin. Solid State Mater. Sci. 24 (2020) (6).
[18] X. Guo, W. Sigle, J. Fleig, J. Maier, Solid State Ionics 154 (2002) 555.
[19] X. Xu, F. Barrows, V.P. Dravid, S.M. Haile, C. Phatak, J. Appl. Phys. 128 (2020) 21.
[20] X. Xu, Y.Z. Liu, J. Wang, D. Isheim, V.P. Dravid, C. Phatak, S.M. Haile, Nat. Mater. 19 (8) (2020) 887.
[21] X. Xu, C. Carr, X.Q. Chen, B.D. Myers, R.Y. Huang, W.Z. Yuan, S. Choi, D.Z. Yi, C. Phatak, S.M. Haile, Adv. Energy Mater. 11 (2021) 10.
[22] C.G. Carr, T. Zhou, M. Cherukara, C. Phatak, S.M. Haile, Mrs Commun 13 (5) (2023) 871.
[23] M. Leonhardt, J. Jamnik, J. Maier, Electrochem. Solid-State Lett. 2 (7) (1999) 333.
[24] M. Halabi, V. Ezersky, A. Kohn, S. Hayun, J. Am. Ceram. Soc. 100 (2) (2017) 800.
[25] M. Vollman, R. Waser, J. Am. Ceram. Soc. 77 (1) (1994) 235.
[26] J. Fleig, S. Rodewald, J. Maier, J. Appl. Phys. 87 (5) (2000) 2372.
[27] C.Y.S. Chang, I. Lubomirsky, S. Kim, Phys. Chem. Chem. Phys. 20 (28) (2018) 19250.
[28] C.Y.S. Chang, I. Lubomirsky, S. Kim, Phys. Chem. Chem. Phys. 20 (13) (2018) 8719.
[29] C.Y.S. Chang, I. Lubomirsky, S. Kim, J. Phys. Chem. C 123 (7) (2019) 4396.
[30] S. Kim, S.K. Kim, S. Khodorov, J. Maier, I. Lubomirsky, Phys. Chem. Chem. Phys. 18 (4) (2016) 3023.
[31] S.K. Kim, S. Khodorov, C.T. Chen, S. Kim, I. Lubomirsky, Phys. Chem. Chem. Phys. 15 (22) (2013) 8716.
[32] S.K. Kim, S. Khodorov, I. Lubomirsky, S. Kim, Phys. Chem. Chem. Phys. 16 (28) (2014) 14961.
[33] S. Rodewald, J. Fleig, J. Maier, J. Eur. Ceram. Soc. 21 (10–11) (2001) 1749.
[34] X. Guo, S.B. Mi, R. Waser, Electrochem. Solid-State Lett. 8 (1) (2005) J1.
[35] I. Riess, J. Electroceram. 17 (2–4) (2006) 247.
[36] D. Kalaev, I. Riess, Solid State Ionics 212 (2012) 26.
[37] I. Riess, J. Maier, Phys. Rev. Lett. 100 (2008) 20.
[38] D.C. Dube, H.J. Scheel, I. Reaney, M. Daglish, N. Setter, J. Appl. Phys. 75 (8) (1994) 4126.
[39] R. Aleksiyko, M. Berkowski, J. Fink-Finowicki, P. Byszewski, R. Diduszko, E. Kowalska, P Soc Photo-Opt Ins 4412 (2001) 50.
[40] E. Makagon, R. Merkle, J. Maier, I. Lubomirsky, Solid State Ionics 344 (2020) (Unsp 115130).
[41] E. Makagon, O. Kraynis, R. Merkle, J. Maier, I. Lubomirsky, Adv. Funct. Mater. 31 (2021) (50) Artn 2104188).
[42] K.D. Kreuer, Solid State Ionics 125 (1–4) (1999) 285.
[43] K.D. Kreuer, S. Adams, W. Münch, A. Fuchs, U. Klock, J. Maier, Solid State Ionics 145 (1–4) (2001) 295.
[44] C.Y.R. Vera, H.P. Ding, D. Peterson, W.T. Gibbons, M. Zhou, D. Ding, Journal of Physics-Energy 3 (2021) 3.
[45] M. Shirpour, R. Merkle, J. Maier, Solid State Ionics 216 (2012) 1.
[46] C.T. Chen, C.E. Danel, S. Kim, J. Mater. Chem. 21 (14) (2011) 5435.
[47] J. Palisaitis, M.E. Ivanova, W.A. Meulenberg, O. Guillon, J. Mayer, J. Eur. Ceram. Soc. 35 (5) (2015) 1517.
[48] H. Fjeld, D.M. Kepaptsoglou, R. Haugsrud, T. Norby, Solid State Ionics 181 (3–4) (2010) 104.
[49] A.D. Brandao, N. Nasani, A.A. Yaremchenko, A.V. Kovalevsky, D.P. Fagg, Int. J. Hydrog. Energy 43 (40) (2018) 18682.
[50] M. Shirpour, R. Merkle, J. Maier, Solid State Ionics 225 (2012) 304.
[51] K.D. Kreuer, Annu. Rev. Mater. Res. 33 (2003) 333.